Structure of the Sr-Zr isotopes near and at the magic $N = 50$ shell from g-factor and lifetime measurements in $^{88}_{40}$Zr and $^{84,86,88}_{38}$Sr

G. J. Kumbartzki,[1] K.-H. Speidel,[2] N. Benczer-Koller,[1] D. A. Torres,[1,*] Y. Y. Sharon,[1] L. Zamick,[1] S. J. Q. Robinson,[3] P. Maier-Komor,[4] T. Ahn,[5] V. Anagnostatou,[5] Ch. Bernards,[5,†] M. Elvers,[5,†] P. Goddard,[5] A. Heinz,[5] G. Ilie,[5] D. Radeck,[5,†] D. Savran,[5,†] V. Werner,[5] and E. Williams[5]

[1]*Department of Physics and Astronomy, Rutgers University, New Brunswick, New Jersey 08903, USA*
[2]*Helmholtz-Institut für Strahlen- und Kernphysik, Universität Bonn, Bonn, Germany*
[3]*Physics Department, Millsaps College, Jackson, Mississippi 39210, USA*
[4]*Physik-Department, Technische Universität München, München, Germany*
[5]*Wright Nuclear Structure Laboratory, Yale University, New Haven, Connecticut 06520, USA*

(Received 15 February 2012; published 27 April 2012)

Background: The evolution of and interplay between single-particle and collective excitations in the $40 \leqslant N \leqslant 50$ range for $_{38}$Sr and $_{40}$Zr isotopes have been studied.
Purpose: Measurement of the g factor of the 2_1^+ and 4_1^+ states in radioactive ^{88}Zr while simultaneously remeasuring the $g(2_1^+)$ factors in the Sr isotopes and extention of the measurements to higher energy states in the Sr isotopes. Lifetimes of states in these nuclei are determined.
Methods: The transient field technique in inverse kinematics and line-shape analysis using the Doppler-shift attenuation method are applied. The ^{88}Zr nuclei were produced by the transfer of an α particle from the ^{12}C nuclei of the target to ^{84}Sr nuclei in the beam. The excited states in the stable ^{84}Sr isotopes were simultaneously populated via Coulomb excitation by ^{12}C in the same target. Coulomb excitation measurements on ^{86,88}Sr were carried out with the same apparatus.
Results: The resulting g factors and $B(E2)$ values of these nuclei reveal similarities between the two chains of Zr and Sr isotopes. Large-scale shell-model calculations were performed within the $p_{3/2}$, $f_{5/2}$, $p_{1/2}$, $g_{9/2}$ orbital space for both protons and neutrons and yielded results in agreement with the experimental data.
Conclusions: In this paper the magnetic moments and lifetimes of several low-lying states in ^{88}Zr and ^{84,86,88}Sr have been measured and compared to large-scale shell-model calculations.

DOI: 10.1103/PhysRevC.85.044322 PACS number(s): 21.10.Ky, 21.10.Tg, 21.60.Cs, 27.50.+e

I. INTRODUCTION

Extensive measurements of g factors and transition probabilities have been carried out in the neighboring $_{38}$Sr and $_{40}$Zr isotopes, as a function of level energy and spin in any one isotope, as a function of neutron number in an isotopic chain or for isotonic pairs [1–7]. These nuclei have $Z = 38$ or 40 and both values are considered as candidates for subshell closure. Their neutron numbers span the region $44 \leqslant N \leqslant 60$, above and below the magic $N = 50$. Consequently, they are expected to exhibit single-particle characteristics, with collective features becoming more important for $N \leqslant 46$ and $N \geqslant 58$.

The isotones ^{86}Sr and ^{88}Zr with $N = 48$ have very similar level schemes (Fig. 1) and decay properties. The $B(E2; 2_1^+ \rightarrow 0_1^+)$ values of each Sr and Zr isotonic pair with $40 \leqslant N \leqslant 60$ are practically identical to each other. The only exception is the current $B(E2; 2_1^+ \rightarrow 0_1^+) = 0.052(16)\ e^2\,\mathrm{b}^2$ literature value, based on the experimental lifetime measurement $\tau = 1.2(4)$ ps [8,9] for ^{88}Zr, which clearly exceeds the systematic trends in both the Sr and Zr nuclei. The $B(E2; 2_1^+ \rightarrow 0_1^+)$ values rise dramatically for both Sr and Zr isotopes below and above $N = 50$. They are fairly constant and extremely small between $N = 46$ and $N = 56$ (see Sec. II D). Skyrme-Hartree-Fock calculations of the intrinsic quadrupole moments of protons and neutrons in Zr isotopes support these findings [10].

The g factors of the low-lying states in the Zr isotopes, in particular, vary widely in both magnitude and sign (Fig. 2). Their behavior often reflects fairly unique neutron and proton configurations for different spin states, as well as for proton and neutron symmetric and mixed-symmetry states with the same spin. The measured g factors of the low-lying 2_1^+ and 4_1^+ states of the stable ^{92,94}Zr isotopes are negative, reflecting the dominance of the $(d_{5/2})_\nu$ configuration [$g(d_{5/2})_\nu = -0.765$]. The positive $g(2_2^+)$ factors in ^{92,94}Zr provide yet another indication of the diversity of configurations in the low-lying excited states and are good examples of the variety of neutron-proton couplings in this mass region [4]. In contrast, in ^{90}Zr, protons are excited to the $g_{9/2}$ orbitals, resulting in a large positive $g(2_1^+)$ factor since $g(g_{9/2})_\pi = +1.510$. Zheng and Zamick [11] showed that the ground state of ^{80}Zr is superdeformed with a high occupancy of $g_{9/2}$ protons. Similarly, ^{90}Zr, although not as deformed as ^{80}Zr, should exhibit a substantial $(g_{9/2})_\pi$ occupancy. The neutron contributions play a minor role due to the rigid $N = 50$ shell closure. A similar feature was found in ^{88}Sr, where the measurements yielded, within the experimental uncertainty, the same positive large $g(2_1^+)$ factor as for its isotonic partner ^{90}Zr [7].

*Current address: Departamento de Física, Universidad Nacional de Colombia, Bogotá, Colombia.
†Institut für Kernphysik, Universität zu Köln, Zülpicher Straße 77, D-50937 Köln, Germany.

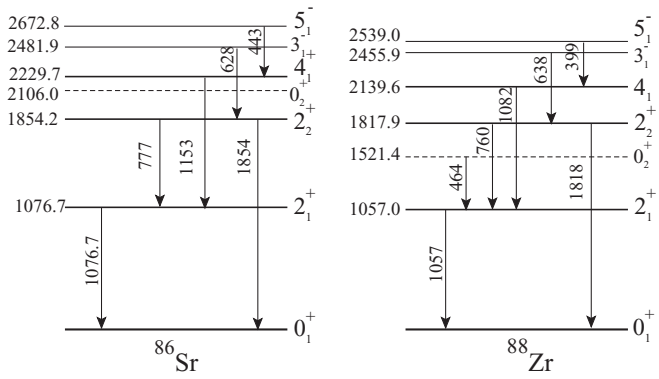

FIG. 1. Energy level diagrams of the low-lying states in ^{86}Sr and ^{88}Zr.

The systematics of the $g(2^+_1)$ factors around mass $A = 80$ have been examined in the framework of IBM-II and shell-model calculations [12].

Thus, the Sr and Zr nuclei offer a natural laboratory in which to study the evolution of nuclear structure across a region near shell closure. Figure 2 displays the g factors for the 2^+_1, 4^+_1, 2^+_2, and 3^-_1 states of $^{84-102}$Zr.

These findings motivated the measurements of lifetimes and g factors in ^{88}Zr and remeasurements in the ^{84,86,88}Sr isotopes [5]. In all cases beams of separated Sr isotopes were used. The ^{88}Zr nuclei were produced with a beam of ^{84}Sr by pickup of α particles from a ^{12}C target. The residual ^{8}Be nuclei break up into two α particles that are subsequently detected. The ^{88}Zr nuclei are unstable and have a half-life of $T_{1/2} =$ 83.4 d. Coulomb excitation of the stable ^{84,86,88}Sr beams by a carbon target was used as the standard approach for the excitation of the Sr isotopes.

II. EXPERIMENTAL TECHNIQUE

The transient field perturbed-angular-correlation technique was used as described in previous papers [13]. Isotopically pure beams of ^{84,86,88}Sr were accelerated at the ESTU tandem accelerator of the Wright Nuclear Structure Laboratory (WNSL) at Yale University, at beam energies ranging from 243 to 285 MeV. The beams scattered off multilayered targets commonly used for this type of experiment.

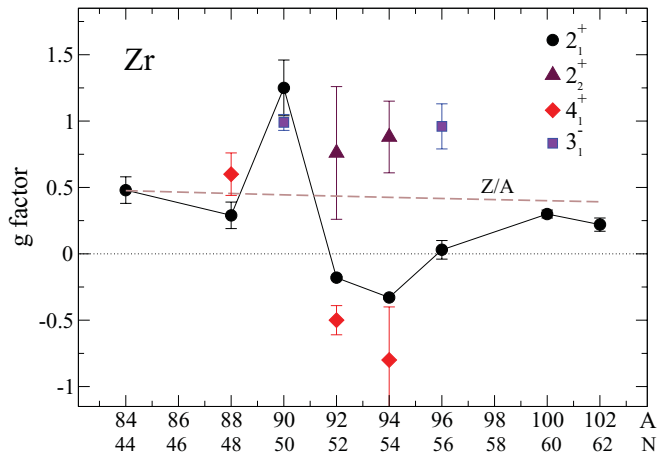

FIG. 2. (Color online) g factors for low-lying states in $^{84-102}$ Zr, obtained from the literature [1–4,7]. The g factors of the 2^+_1 and 4^+_1 states in ^{88}Zr were obtained in the present work.

A. ^{84}Sr beam preparation

For these investigations, and especially for the production of ^{88}Zr, abundant and isotopically pure Sr beams were required. The ^{84}Sr beam was prepared from material enriched to 48.85%, while the ^{86,88}Sr beams were made using natural Sr. Negatively charged Sr compounds were prepared in the form of hydrides for injection into the Tandem accelerator. Considerable developmental work was required to optimize various delicate chemical and physical procedures, in particular in consideration of the high cost of the isotopically enriched ^{84}Sr.

The procedure started with 170 mg of $^{84}SrCO_3$. Half of this amount was mixed with 255 mg of ZrH_2 in a 1:3 proportion. The mixture was heated in a Ta crucible under vacuum, to about 600–900 °C, to boil off the H_2 and the CO_2. Once the vacuum was recovered, the heating of the sample was continued to an estimated 1700 °C to cause the reaction $2SrO + Zr \rightarrow 2\,Sr + ZrO_2$ and to boil off the Sr. About 50% of the ^{84}Sr was recovered, collected on a water-cooled plate above the heated crucible and transferred in an Ar atmosphere to a Vycor tube. The tube was heated to about 700 °C in 600 Torr of hydrogen to create SrH_2, which was finally transferred to the sputter cone in an Ar-filled glove box.

B. Target composition and magnetization

Three targets were used for these experiments. Their compositions are shown in Table I. In target I, the C was evaporated onto the gadolinium layer. The Ta layer was used in the preparation of the gadolinium layer and also ensured good adhesion of the copper layer. In Targets II and III, the C layer was brushed from a colloidal graphite suspension onto rolled and annealed foils of gadolinium or iron, which were also backed by a copper layer. Target III with the iron layer was used to compare the results obtained in the current experiments with those described in the literature [5].

The targets were mounted on the tip of a Displex closed-cycle refrigerator and cooled to approximately 50 K. During the experiment the ferromagnetic layer was magnetized by an external field of 0.07 T, applied perpendicularly to the reaction

TABLE I. Compositions and thicknesses (mg/cm^2) of the different targets used in this experiment. The magnetization, $\vec{M}$, is quoted in tesla.

Target	C	Gd	Ta	Cu	$\vec{M}$ (T)
I	0.606	6.426	1.0	5.6	0.1780
II	0.4	4.40		7.8	0.1650
		Fe			
III	0.45	4.45		4.9	0.1749

plane. The external field direction was reversed approximately every 100 s.

The magnetizations, $\vec{M}$, of the targets were measured offline before the experiment with the Rutgers AC magnetometer [14] as a function of the applied external field and were found to be approximately constant at temperatures between 50 and 100 K. The iron-based target was used both at room temperature and in the refrigerated mode.

The excited reaction products, ^{88}Zr or ^{84,86,88}Sr isotopes, traversed the ferromagnetic foil and were stopped in the copper backing. The beam was stopped in additional copper foils totaling 11.2 mg/cm^2, which were placed between the target and the particle detector.

C. Detector array geometry

The ^{12}C ions scattered in the Coulex interactions with the beam, as well as residual α particles produced in the α-transfer reaction, were detected in a circular Si detector (Canberra PIPS). The detector was 100 μm thick, had a radius of 9.5 mm, was located 30 mm downstream from the target, and subtended an angle of $\pm 18^\circ$ with respect to the beam axis.

The γ rays resulting from either the Coulomb excitation or the α-transfer reaction were detected by four segmented clover detectors mounted in the horizontal plane at a distance of 132 mm from the target. They were shielded from low-energy γ and x rays by a combination of thin copper/cadmium/lead absorbers. For the precession measurements, the clover detectors were positioned at angles of $\pm 67^\circ$ and $\pm 113^\circ$ with respect to the beam axis.

All of the detector signals were digitally processed by PIXIE-4 electronic modules [15] and recorded as singles events. Particle-γ coincidence events were later selected according to their time information. The signals from each of the four elements of a clover detector were processed separately. Compton add-back was performed for each element. The data were subsequently combined for further analysis either in groups of four elements representing the whole clover detector at some angle θ or in two groups of two elements each located at a nominal angle of $\theta \pm 8^\circ$.

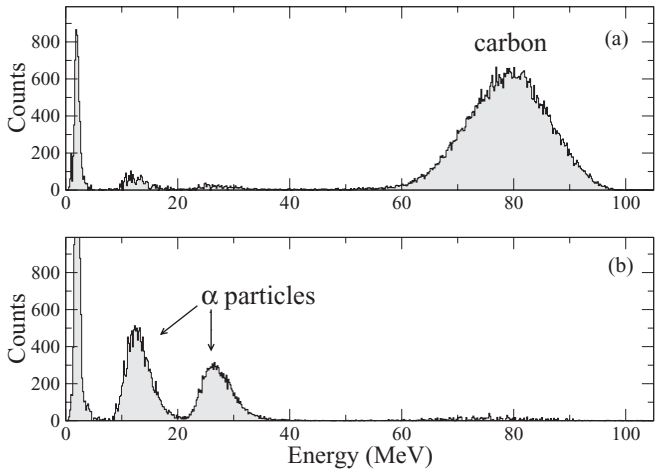

FIG. 3. Coincident particle spectra: (a) gated by ^{84}Sr γ rays and (b) gated by ^{88}Zr γ rays ($E_{\mathrm{BEAM}} = 275$ MeV).

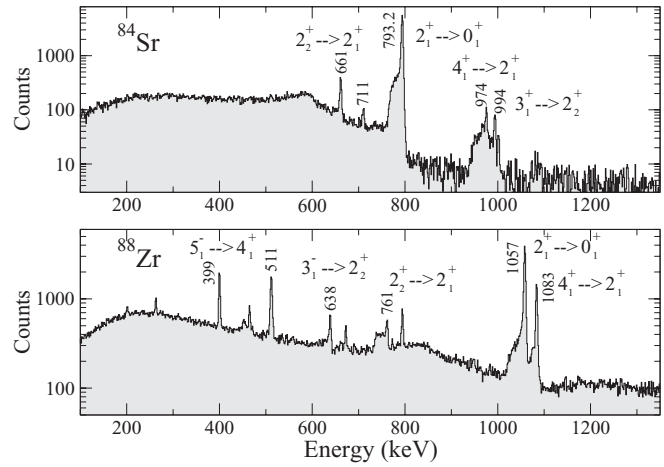

FIG. 4. Gamma spectra gated by ^{12}C ions (top: ^{84}Sr) and α particles (bottom: ^{88}Zr) in a detector positioned at an angle of 113° and for a beam energy of 275 MeV.

The α-transfer reaction occurs only at beam energies close to, or above, the Coulomb barrier for the projectiles and the C nuclei of the target. Above the Coulomb barrier, fusion-evaporation reactions become dominant and flood the Si particle detector with light particles. These particles are not stopped in the thin detector but produce low-energy dE/dx signals. At the same time, at higher energies the Coulomb excitation channel is increasingly suppressed while the α-transfer cross section remains fairly constant.

Selected particle spectra are shown in Fig. 3. By gating on the γ rays of ^{84}Sr or ^{88}Zr the clear separation of the particle groups is shown. The corresponding γ spectra resulting from the particle selection are displayed in Fig. 4. Similar spectra for ^{86}Sr and ^{88}Sr are shown in Fig. 5.

D. Spectroscopy of the ^{88}Zr and ^{84,86,88}Sr isotopes

The thrust of the experiments described in this paper was to measure magnetic moments. In transient-field measurements

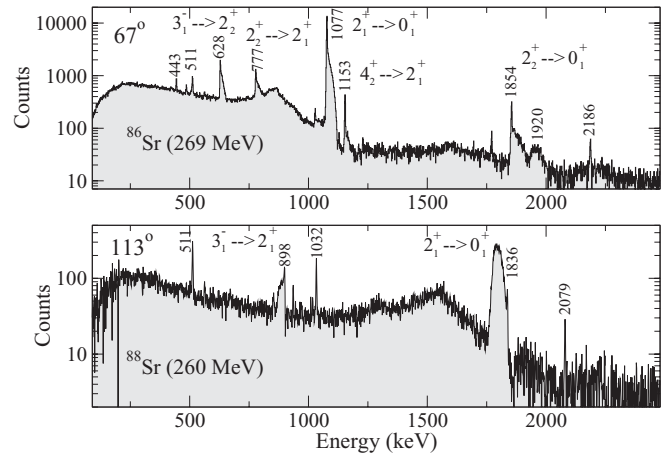

FIG. 5. Full-clover γ-spectra of ^{86}Sr (top) and ^{88}Sr (bottom) gated by ^{12}C ions at the given beam energies.

TABLE II. Relative feeding intensities in ^{88}Zr following the α-transfer reaction.

$2_1^+ \to 0_1^+$	$0_2^+ \to 2_1^+$	$2_2^+ \to 2_1^+$	$4_1^+ \to 2_1^+$	$3_1^- \to 2_2^+$	$5_1^- \to 4_1^+$
100	5	14	33	9	15

the magnetic interaction happens only for those excited states the nucleus is in while traversing the ferromagnetic medium. If higher excited states are populated, their spin precessions are preserved in the subsequent decays and are accumulated in the precession of the lower states. A knowledge of the decay histories of the nuclei is then needed to interpret the measured precessions.

In the α-transfer reaction, states at higher excitation energies are populated and decay to the lower states via multiple paths. Table II shows relative feeding intensities observed in ^{88}Zr in this experiment. Since the lifetimes of the feeding states are rarely known and since most transition intensities are small, as was shown in Ref. [16], the feeding corrections have little effect on the final g factors of the lower states and are well within the quoted errors. In Coulomb excitation, excited states are populated from the ground up by well-defined excitation processes. Higher excited states require higher beam energies. Therefore, feeding can be largely controlled by choosing the beam energy. Table III shows typical kinematic parameters for the reactions used in the excitation of the 2_1^+ states.

1. Measurements of lifetimes by the Doppler shift attenuation method

In inverse kinematic reactions the excited nuclei have high recoil velocities. While these nuclei slow down and stop in the target, their γ-decay lines exhibit line shapes suitable for the determination of lifetimes for the decaying states. The LINESHAPE code [17] was used. The Monte Carlo calculation of the decay histories was modified to take into account multilayer targets [18]. In all cases the stopping power tabulation of Ziegler *et al.* [19] was used.

The measured lifetimes are listed in Table IV together with the previously known values reported in the literature [9]. Examples of line-shape fits are shown in Figs. 6– 8.

Of special interest was the lifetime of the 2_1^+ state in ^{88}Zr. The quoted $B(E2; 2_1^+ \to 0_1^+)$ literature value was much larger than that of the neighboring isotopes. The 2_1^+ state is fed by the 4_1^+ state, which in turn is fed in the decay of a 5^- state. The decay γ rays of the 5_1^- state show no discernible line shape indicating a longer lifetime. Therefore, the 4_1^+ state was first fitted separately by taking into account a stopped component representing the feeding from the 5_1^- state. This procedure resulted in a lifetime $\tau = 2.2(2)$ ps for the 4_1^+ state for which no prior lifetime measurement existed. With this value fixed, the $4_1^+ \to 2_1^+$ and $2_1^+ \to 0_1^+$ transitions were fitted as a cascade, as shown in Fig. 6 for the two half-clover segments. Both fits yield a lifetime for the 2_1^+ state of 3.6(3) ps, much larger than the prior value of 1.20(4) ps.

In the Sr isotopes the lifetimes of the 2_1^+ states were determined from data taken at beam energies such that feeding from higher states was negligible (Fig. 7). Feeding had to be considered at the higher beam energies needed to excite higher states. For example, higher states in ^{84}Sr are close in energy and decay into each other (Fig. 8). The lifetime of the 4_1^+ state could not be determined reliably in spite of a good-looking fit. According to the partial level scheme of ^{84}Sr in Fig. 9, the 5_1^- state decays with a relative long lifetime of 13.7(9) ps [22] to the 4_1^+ state. A branch of the 3_1^- state decaying via a 994-keV γ ray is unresolved from the 974-keV transition. Nevertheless, various fitting attempts consistently yielded a lifetime of less than 1 ps for the 4_1^+ state, which is much shorter than the current literature value.

In ^{86}Sr the lifetime fit of the 2_2^+ state gave the same value as for the feeding 3_1^- state and could therefore not be determined either. Most of the results obtained are in fair agreement with the literature values, except for the aforementioned discrepancy observed for $\tau(2_1^+, ^{88}\text{Zr})$. The new value is a factor of 3 larger than the one previously quoted. The resulting $B(E2; 2_1^+ \to 0_1^+)$ value in ^{88}Zr is now in better agreement with the systematics in the Sr and Zr isotopes, as shown in Fig. 10. Table IV shows E_I, I_i^π, lifetimes, and $(BE2; I_i \to I_f)$ values from the literature and this work. Several lifetimes were obtained in spite of the fact that the analysis is sensitive to correlated parameters which are not always precisely known.

2. Spin alignment and angular correlation measurements

The Coulomb excitation and α-transfer reactions produce different spin alignments and hence different angular correlations. Coulomb-excitation studies yield a pronounced angular

TABLE III. Kinematics for the α-transfer and Coulomb-excitation reactions leading to the 2_1^+ states of the ^{88}Zr and ^{84,86,88}Sr nuclei for target I. Similar values are obtained for targets II and III. The $\langle E\rangle_{\text{in}}$ and $\langle E\rangle_{\text{out}}$ values and $\langle v/v_0\rangle_{\text{in}}$ and $\langle v/v_0\rangle_{\text{out}}$ values are, respectively, the average energies and velocities of the excited ions as they enter into and exit from the gadolinium layer, and $v_0 = e^2/\hbar$ is the Bohr velocity. T is the effective transit time of the ions through the ferromagnetic layer. This effective transit time accounts for the early decay of short-lived states.

Probe ions	E_{beam} (MeV)	$\langle E\rangle_{\text{in}}$ (MeV)	$\langle E\rangle_{\text{out}}$ (MeV)	$\left\langle \frac{v}{v_0}\right\rangle_{\text{in}}$	$\left\langle \frac{v}{v_0}\right\rangle_{\text{out}}$	T (ps)
^{88}Zr	275	175.3	48.2	9.0	4.7	0.518
^{84}Sr	275	138.4	30.0	8.0	3.6	0.608
^{86}Sr	250	121.5	21.0	7.6	3.1	0.604
^{88}Sr	270	135.5	28.5	7.9	3.6	0.147

TABLE IV. Results of lifetime measurements. Listed are level energy E_x, spin and parity, mean lifetimes, and $B(E2; I_i \to I_f)$ in $e^2\,b^2$. The $B(E2; I_i \to I_f)$ values were calculated using the two interactions JJ4B [20] and JUN45 [21] using the effective charge values $e_p = 1.5e$ and $e_n = 0.5e$.

Nucleus	E_x	I^π	Transition	τ (ps)		$B(E2; I_i \to I_f)_{exp}$		$B(E2; I_i \to I_f)_{th}$	
	(MeV)		$I_i \to I_f$	Refs. [5,9,22,23]	This work	Refs. [5,9,22,23]	This work	JJ4B	JUN45
^{88}Zr									
	1.057	2_1^+	$2_1^+ \to 0_1^+$	1.20(4)	3.6(4)	0.052(16)	0.017(2)	0.0346	0.0192
	1.818	2_2^+	$2_2^+ \to 0_1^+$	0.30(13)	0.81(10)	–[a]	0.0018(2)	0.00001	0.0016
			$2_2^+ \to 2_1^+$		0.89(10)		0.0024(2)	0.0303	0.0218
	2.140	4_1^+	$4_1^+ \to 2_1^+$		2.2(2)		0.025(2)	0.0615	0.0331
	2.456	3_1^-	$3_1^- \to 2_2^+$		2.8(3)				
^{84}Sr									
	0.793	2_1^+	$2_1^+ \to 0_1^+$	4.66(50)	4.2(2)	0.056(6)	0.062(3)	0.053	0.034
	1.768	4_1^+	$4_1^+ \to 2_1^+$	2.0(6)	< 1	0.046(14)		0.080	0.049
	2.448	3_1^-	$3_1^- \to 2_1^+$		1.4(1)	–[a]			
^{86}Sr									
	1.077	2_1^+	$2_1^+ \to 0_1^+$	2.32(10)	2.0(1)	0.024(1)	0.028(1)	0.0269	0.0201
	1.854	2_2^+	$2_2^+ \to 0_1^+$	0.557(29)	–	0.0029(1)		0.0325	0.0215
	2.230	4_1^+	$4_1^+ \to 2_1^+$	<5	2.5(3)		0.016(2)	0.0352	0.0193
	2.482	3_1^-	$3_1^- \to 2_2^+$	<5	1.3(1)				
^{88}Sr									
	1.836	2_1^+	$2_1^+ \to 0_1^+$	0.213(11)	0.219(18)	0.018(1)	0.018(1)	0.0171	0.0142
	2.734	3_1^-	$3_1^- \to 2_1^+$	1.12(7)	0.97(4)				

[a]Branching and/or mixing ratios are not known

correlation of the decay γ rays with respect to the beam direction. The α-transfer reaction yields a relatively small degree of alignment and therefore weaker angular correlations [16]. The slopes of the angular correlations presented in Table V were obtained by at least one of three techniques: (a) measurements with a γ detector moving over the angular range of 35° to 90°, (b) the γ-ray intensity ratios observed in detectors located alternatively at different angles, or (c) the anisotropy ratio from the two independent halves of the clover detectors using the data of the precession measurements. All the methods give compatible results.

E. Precession measurements and determination of *g* factors

The precession angle $\Delta\theta$ of the angular correlation was measured from the change in counting rates in detectors placed at specific angles with respect to the beam direction, as was described, for instance, in Ref. [13]. The essential quantities, such as the logarithmic slopes and precession angles, together with the derived g factors, are summarized in Table V.

$\Delta\theta(g = 1)$ is calculated using

$$\Delta\theta = -g\frac{\mu_N}{\hbar}\int_{t_{in}}^{t_{out}} B_{TF}[v(t), Z]e^{-t/\tau}dt, \qquad (1)$$

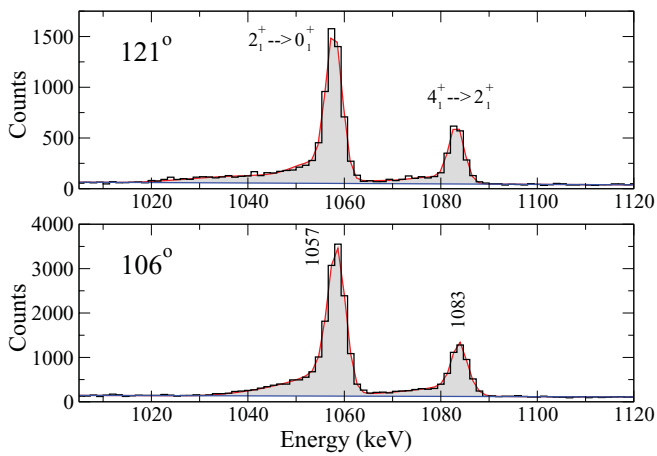

FIG. 6. (Color online) Line shapes of the $2_1^+ \to 0_1^+$ and the $4_1^+ \to 2_1^+$ transitions in ^{88}Zr, superposed on the best fit obtained by the DSAM technique.

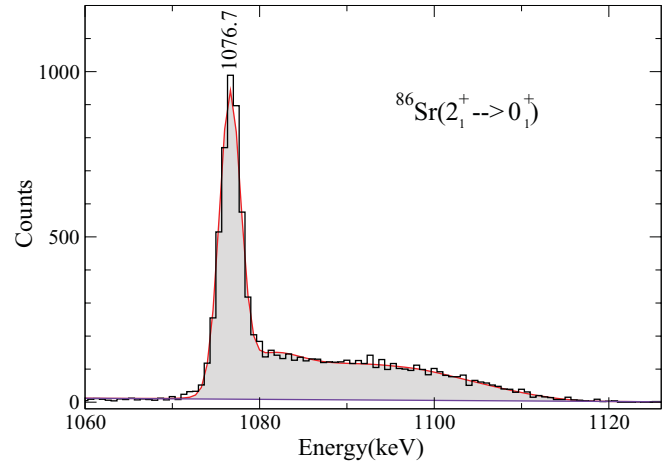

FIG. 7. (Color online) The line-shape fit for the $2_1^+ \to 0_1^+$ transition in ^{86}Sr. The data were taken at 243 MeV where only the 2_1^+ state is excited.

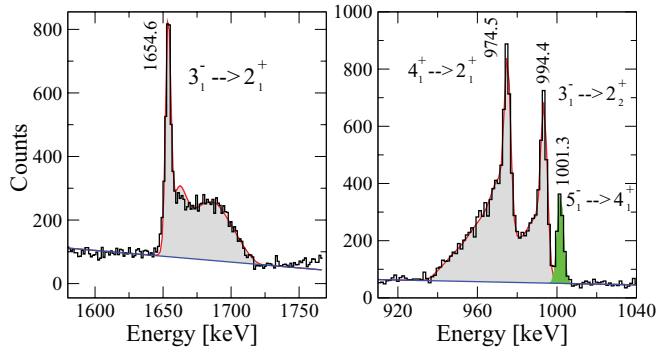

FIG. 8. (Color online) Line shapes of the $3^-_1 \rightarrow 2^+_1$, the $4^+_1 \rightarrow 2^+_1$, and the $3^-_1 \rightarrow 2^+_2$ transitions in ^{84}Sr (see also text). The spectra are from clover segments at 59° and 121°.

where the field strength

$$B_{\mathrm{TF}}[(v(t), Z] = aZ^{1.1}(v/v_0)^{0.45}\vec{M} \qquad (2)$$

is taken from the Rutgers parametrization [24].

III. RESULTS

Tables IV–VI include the experimental results of the present investigations as well as the results of large-scale shell-model calculations using the two different interactions JJ4B [20] and JUN45 [21].

A. $B(E2)$ values

Table IV displays the experimental $B(E2)$ values obtained in this work from the lifetime determinations and the shell-model calculation results. Figure 10 shows the systematics of $B(E2)$ values for the $2^+_1 \rightarrow 0^+_1$ transitions in the Sr and Zr isotopes near $N = 50$ including the new result for ^{88}Zr.

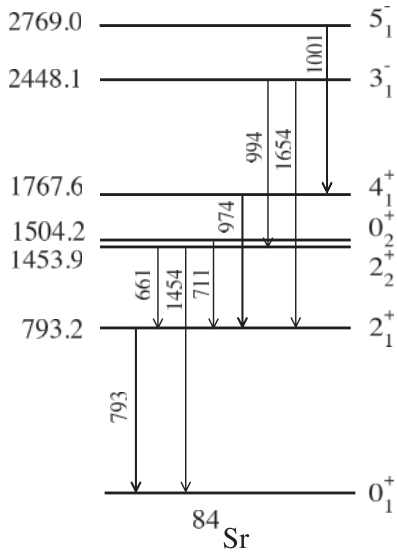

FIG. 9. Partial level diagram of ^{84}Sr.

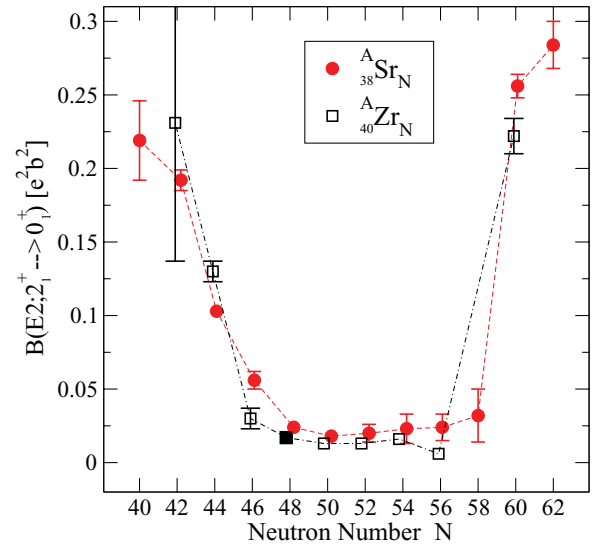

FIG. 10. (Color online) Summary of $B(E2; 2^+_1 \rightarrow 0^+_1)$ values for the even Zr and Sr isotopes near $N = 50$. The solid square is the $B(E2)$ value derived from the lifetime determined for ^{88}Zr in the present experiment. The lines are drawn to guide the eyes.

B. g factors

Table V shows the experimental g factors determined for various states in ^{88}Zr and in ^{84,86,88}Sr, as well as previous literature values and the results of shell-model calculations. Measurements were carried out on different targets, and at different energies. Most of the data were taken with target I at the energies given in Table III. The quoted g factors include results from measurements at the other beam energies. The results for targets II and III are shown separately.

The Sr data for the 2^+_1 states are in good agreement with the results of previous measurements carried out in normal kinematics and with iron ferromagnetic targets [5]. The ^{88}Zr g factor data for the 2^+_1 and 4^+_1 states and the g factors for higher spin states in the Sr isotopes are new. The sign of the $g(4^+_1)$ state in ^{86}Sr was measured to be negative. This observation is reinforced by the opposite precession measured for the $2^+_1 \rightarrow 0^+_1$ transition in the same spectra. Furthermore, the background under the 1153-keV γ line exhibits a small positive precession. Unfortunately, during the very last run at the Yale tandem, the beam energy could not be raised enough to increase the excitation of the 4^+_1 state. Only about 700 counts per field direction and detector were accumulated, effectively limiting the precision of the obtained g factor. Figure 11 shows the systematics of $g(2^+_1)$ factors in Sr and Zr isotopes near $N = 50$ including the newly determined g factor for ^{88}Zr with $N = 48$.

C. Excitation energies

Table VI compares the experimental energies of the excited states with the results of the shell-model calculations for ^{88}Zr and ^{84,86,88}Sr.

TABLE V. Summary of all the g values obtained for the Zr and Sr isotopes. The theoretical results are calculated using the free-nucleon g factors.

Nucleus	I^π	$\lvert S(67^\circ)\rvert$	$\lvert\Delta\theta\rvert$	$\Delta\theta(g=1)$	g factors		Theory		
		(mrad^{-1})	(mrad)	(mrad)	Ref. [5]	This work	JJ4B	JUN45	JUN45 [21]
^{88}Zr									
	2_1^+	0.50(8)	17.6(60)	56.0		+0.30(11)	+0.77	+0.39	
	2_2^+						+0.31	+0.54	
	4_1^+	0.55(4)	36.3(98)	55.8		+0.65(18)	+0.84	+0.49	
^{84}Sr									
	2_1^+	2.11(1)	28.4(3)	59.2	+0.419(47)	+0.48(1)			+0.35
^{86}Sr									
	2_1^+	2.07(4)	15.0(2)	52.6	+0.273(50)	+0.285(14)	+0.38	+0.28	+0.29
		2.22(6)	13.4(20)	41.5		+0.323(51)[a]			
	2_2^+	1.77(13)	22.0(85)	55.0		+0.40(16)	+0.36	+0.30	
	4_1^+	0.805(11)	39.3(280)	57.8		− 0.68(49)	+0.22	− 0.07	
^{88}Sr									
	2_1^+	2.19(2)	18.4(26)	15.1	+1.15(17)	+1.22(11)	+1.00	+1.15	+1.15
	2_1^+	1.98(3)	15.8(411)	14.4		+1.17(31)[b]			

[a]Target III: with iron as ferromagnetic material (243 MeV).
[b]Target II: one run at 260 MeV.

IV. THEORETICAL CALCULATIONS

A. Shell-model calculations

The $_{38}$Sr and $_{40}$Zr isotopes are of special interest because of possible subshell closures at $Z = 38$ and $Z = 40$. Furthermore, one would expect a single-particle picture to apply as N approaches 50 from above and below and collective effects to play an increasing role as N moves further away from 50. The above picture is also suggested by the relatively small $B(E2; 2_1^+ \rightarrow 0_1^+)$ values in the Sr and Zr isotopes with N near 50. Large-scale shell-model calculations have been carried out using the shell-model code ANTOINE [25]. The shell-model space that was used consisted of the single-particle orbitals $1p_{3/2}$, $0f_{5/2}$, $1p_{1/2}$, and $0g_{9/2}$, for both protons and neutrons. Two residual interactions were used, JJ4B of Lisetskiy *et al.* [20] and JUN45 of Honma *et al.* [21]. Four nuclei were considered: ^{88}Zr, and ^{84,86,88}Sr. The calculated results are shown in Tables IV–VI.

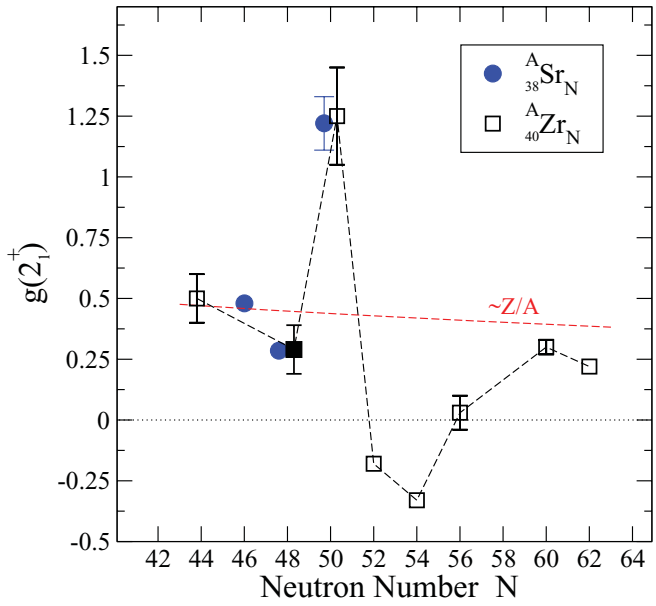

FIG. 11. (Color online) Summary of $g(2_1^+)$ factors for the Zr and Sr isotopes near $N = 50$. The open symbols are data from Ref. [9]; the solid symbols are data from this work. Lines are drawn to guide the eyes.

B. A comparison of the $N = 48$ isotones ^{88}Zr and ^{86}Sr

The experimental spectroscopic properties of these two nuclei are in some respects very similar. Their excitation

TABLE VI. Experimental level energies in MeV and results of theoretical calculations.

Nucleus	I^π	E_x	Theory	
		(exp)	JJ4B	JUN45
^{88}Zr				
	2_1^+	1.057	0.99	1.18
	2_2^+	1.818	1.87	1.77
	4_1^+	2.140	2.09	2.29
^{84}Sr				
	2_1^+	0.793	0.678	0.850[a]
	2_2^+	1.454	1.374	1.846
	4_1^+	1.768	1.621	1.919
^{86}Sr				
	2_1^+	1.077	1.136	1.178
	2_2^+	1.854	2.035	1.998
	4_1^+	2.230	2.458	2.462
^{88}Sr				
	2_1^+	1.836	1.858	1.83[a]

[a]The same values were also obtained in Ref. [21]

energies differ by 20 keV for the 2_1^+ states, 36 keV for the 2_2^+ states, and 90 keV for the 4_1^+ levels. The two g factors, $g(^{88}\mathrm{Zr};2_1^+) = +0.30(11)$ and $g(^{86}\mathrm{Sr};2_1^+) = +0.29(1)$, are the same. One possible explanation for the similarities of the properties of these two isotopes is that the two additional protons in ^{88}Zr may fill the $p_{1/2}$ subshell. These protons may thus close the $p_{1/2}$ subshell and therefore do not contribute to the magnetic moments of ^{88}Zr.

Overall, the calculations of excitation energies, $B(E2)$ values, and g factors carried out with the JUN45 interaction for both ^{88}Zr and ^{86}Sr yield results which agree well with the experimental data (Tables IV–VI). For the measured g factors of both ^{88}Zr and ^{86}Sr all the values calculated with the JUN45 interaction agree with the experimental results within their errors. The calculated g factor results using the JJ4B interaction show somewhat less agreement. The average deviation of the excitation energy prediction for both nuclei and with both interactions is within about 105 keV of the experimental values; with JJ4B for ^{88}Zr the corresponding value is 57 keV. The $B(E2)$ value predictions are often fairly close for both interactions and for both nuclei.

The close agreement between the calculated shell-model results and the experimental values for both $^{88}_{40}\mathrm{Zr}_{48}$ and $^{86}_{38}\mathrm{Sr}_{48}$ is not surprising. Both of these $N = 48$ isotones are only two neutron holes away from the $N = 50$ shell closure and have proton numbers, 40 and 38, often considered as candidates for subshell closure. Hence, one would expect the shell model to work well.

C. The negative value of the $g(4_1^+)$ of ^{86}Sr

The current work reports the first measurement of a $g(4_1^+)$ factor for any Sr isotope, namely, for ^{86}Sr, and this value is negative. In contrast, $g(^{88}\mathrm{Zr};4_1^+)$ is positive.

There are only three orbitals for which the single-particle Schmidt values for the g factors are negative in the shell-model space under consideration. For the protons, only $g(p_{1/2})_\pi = -0.529$ is negative. It is hard to think of a simple proton configuration of positive parity that couples to a 4^+ state and has a negative g factor. For the neutrons, the negative Schmidt values are $g(g_{9/2})_\nu = -0.425$ and $g(p_{3/2})_\nu = -1.275$. Thus, possible neutron configurations for the 4_1^+ state which may have a negative g factor are $g(g_{9/2})_\nu^2$ or $g(p_{3/2}, f_{5/2})_\nu$. The Schmidt value for a $f_{5/2}$ neutron is $g(f_{5/2})_\nu = +0.547$. Interestingly, for ^{86}Sr the JUN45 calculation predicts a small negative $g(^{86}Sr;4_1^+) = -0.07$ while the calculation with the JJ4B interaction predicts $g(4_1^+) = +0.22$.

A study of the resulting JUN45 4_1^+ wave function for ^{86}Sr shows it to be very fractionated. But the largest, of many, shell-model configuration in it, with about 20% probability, has a closed $(f_{5/2})^6(p_{3/2})^4$ proton core and the two neutron $g_{9/2}$ holes coupling to 4^+. As expected, this configuration has $g = -0.425$, which is equal to the $g(g_{9/2})_\nu$ Schmidt value.

The largest configuration in the JJ4B 4_1^+ wave function, about 20% in intensity, has two $g_{9/2}$ neutron holes and two protons excited from the $f_{5/2}$ orbit to the $g_{9/2}$ orbit. The g factor of that configuration is calculated to be $+0.784$.

Of course, considering only the largest, nondominant, configuration of a fractionated wave function is suggestive but is hardly a complete explanation for the negative sign of the $g(4_1^+)$ of ^{86}Sr.

D. ^{88}Sr

A simple picture for the 2_1^+ state of $^{88}_{38}\mathrm{Sr}_{50}$ consists of a closed neutron $N = 50$ core and the excitation of two protons from the $f_{5/2}$ orbit to the $g_{9/2}$ orbit. This state would have a large positive g factor. Indeed, such a result was obtained experimentally and was predicted with both the JJ4B and JUN45 interaction calculations (Table V).

For the nearly doubly magic ^{88}Sr nucleus the observed 2_1^+ state excitation energy is high (1.836 MeV), a value well predicted by the calculations. The $B(E2; 2_1^+ \rightarrow 0_1^+)$ value measured in the present investigation, $0.018\ e^2\,\mathrm{b}^2$, is identical to the adopted value [9] and is the smallest such observed value in the even Sr isotopes. Both interactions predict it well.

E. ^{84}Sr

With as many as four neutron holes away from the $N = 50$ shell closure ^{84}Sr is more collective than the other Sr isotopes studied here. Its 2_1^+ excitation energy at 0.793 MeV is the lowest and its $B(E2; 2_1^+ \rightarrow 0_1^+)$ value is the largest. In ^{84}Sr all the excitation energies are predicted within 147 keV by calculations with the JJ4B interaction. The $g(2_1^+)$ value that is calculated with JUN45 is in reasonable agreement with the observed value of 0.48. Calculations carried out with the JJ4B interaction predict the $B(E2; 2_1^+ \rightarrow 0_1^+)$ value to within 15% of the measured value.

V. SUMMARY

In this paper the magnetic moments and lifetimes of several low-lying states in ^{88}Zr and ^{84,86,88}Sr have been measured. The data on ^{88}Zr, a radioactive nucleus for which no target or beam exists, have been obtained for the first time. The approach used involved an α-transfer reaction in which an α particle is transferred from a ^{12}C target to ions in a beam of ^{84}Sr.

The Sr isotopes were excited in this experiment via Coulomb excitation, in inverse kinematics, using gadolinium as ferromagnetic medium. The $g(2_1^+)$ factors thus obtained are in good agreement with earlier results from measurements using iron as the ferromagnetic layer in normal kinematics. In addition, g factors and lifetimes of higher excited states, including 4_1^+, 2_2^+, and 3_1^-, were measured for the first time.

Large-scale shell-model calculations were carried out with a space that included the $1p_{3/2}$, $0f_{5/2}$, $1p_{1/2}$, and $0g_{9/2}$ orbitals for both protons and neutrons. The JJ4B and JUN45 interactions were used and the results were compared. The JUN45 interaction yields g factors and $B(E2)$ values that are in better agreement with the experimental data while the JJ4B interaction predicts the level energies slightly better.

The g factors and $B(E2)$ values of all these nuclei fit well with the systematics in this region. It is noteworthy that the

g factor of the 4_1^+ state in ^{86}Sr has a negative sign, a clear indication of the single-particle neutron-dominated structure of this state.

ACKNOWLEDGMENTS

The authors wish to thank Jeff Ashenfelter and Craig Miller from the WNSL at Yale University for developing the procedure to prepare the ^{84}Sr beam. Targets II and III were based on foils prepared by A. E. Stuchbery from the Australian National University. K.-H.S. acknowledges support by the DFG under SP 190/17-1. Y.Y.S. is grateful for an R&PD grant from Stockton College. D.R. and D.S. thank the German Academic Exchange Service (DAAD) for financial support. We also acknowledge support from the National Science Foundation and the US Department of Energy Grant No. DE-FG02-91ER-40609 to Yale University.

[1] G. Jakob, N. Benczer-Koller, J. Holden, G. Kumbartzki, T. J. Mertzimekis, K.-H. Speidel, C. W. Beausang, and R. Krücken, Phys. Lett. B **468**, 13 (1999).
[2] G. Jakob, N. Benczer-Koller, J. Holden, G. Kumbartzki, T. J. Mertzimekis, K.-H. Speidel, R. Ernst, P. Maier-Komor, C. W. Beausang, and R. Krücken, Phys. Lett. B **494**, 187 (2000).
[3] G. Kumbartzki *et al*., Phys. Lett. B **562**, 193 (2003).
[4] V. Werner *et al*., Phys. Rev. C **78**, 031301(R) (2008).
[5] A. I. Kucharska, J. Billowes, and M. A. Grace, J. Phys. G **14**, 65 (1988).
[6] ENDSF, [http://www.nndc.bnl.gov/nndc/ensdf/].
[7] N. J. Stone, Table of Nuclear Magnetic Dipole and Electric Quadrupole Moments, IAEA Nuclear Data Section INDC(NDS)-0594, 2011.
[8] W. Beens, Ph.D. thesis, Vrije University, Amsterdam, 1973.
[9] G. Mukherjee and A. A. Sonzogni, Nucl. Data Sheets **105**, 419 (2005).
[10] P. Bonche, R. Flocard, P. H. Heenen, S. J. Krieger, and M. S. Weiss, Nucl. Phys. A **443**, 39 (1985).
[11] D. C. Zheng and L. Zamick, Phys. Lett. B **266**, 5 (1991).
[12] T. J. Mertzimekis, A. E. Stuchbery, N. Benczer-Koller, and M. J. Taylor, Phys. Rev. C **68**, 054304 (2003).
[13] G. Gürdal *et al*., Phys. Rev. C **82**, 064301 (2010).
[14] A. Piqué, J. M. Brennan, R. Darling, R. Tanczyn, D. Ballon, and N. Benczer-Koller, Nucl. Instrum. Methods Phys. Res., Sect. A **279**, 579 (1989).
[15] X-Ray Instrumentation Associates, [http://www.xia.com/].
[16] D. A. Torres *et al*., Phys. Rev. C **84**, 044327 (2011).
[17] J. C. Wells and N. R. Johnson, computer code LINESHAPE, PD-LNL version, 1999.
[18] R. Ernst *et al*., Phys. Rev. C **62**, 024305 (2000).
[19] F. J. Ziegler, J. Biersack, and U. Littmark, *The Stopping and Range of Ions in Solids*, Vol. 1 (Pergamon, Oxford, 1985).
[20] A. F. Lisetskiy, B. Brown, M. Horoi, and H. Grawe, Phys Rev. C **70**, 044314 (2004).
[21] M. Honma, T. Otsuka, T. Mizusaki, and M. Hjorth-Jensen, Phys. Rev. C **80**, 064323 (2009).
[22] D. Abriola *et al*., Nuclear Data Sheets **110**, 2815 (2009).
[23] B. Singh, Nucl. Data Sheets **94**, 1 (2001).
[24] N. K. B. Shu, D. Melnik, J. M. Brennan, W. Semmler, and N. Benczer-Koller, Phys. Rev. C **21**, 1828 (1980).
[25] E. Caurier, computer code ANTOINE, IReS, Strasbourg, 1989–2004.